Electrochemical deposition of gold on indium zirconate (InZrOx with In/Zr atomic ratio 1.0) for high temperature automobile exhaust gas sensors

Adeel Afzal, Mike Andersson, Cinzia Di Franco, Nicoletta Ditaranto, Nicola Cioffi, Gaetano Scamarcio, Anita Lloyd Spetz and Luisa Torsi

The original publication is available at www.springerlink.com:

Adeel Afzal, Mike Andersson, Cinzia Di Franco, Nicoletta Ditaranto, Nicola Cioffi, Gaetano Scamarcio, Anita Lloyd Spetz and Luisa Torsi, Electrochemical deposition of gold on indium zirconate (InZrOx with In/Zr atomic ratio 1.0) for high temperature automobile exhaust gas sensors, 2015, Journal of Solid State Electrochemistry, (19), 9, 2859-2868.
http://dx.doi.org/10.1007/s10008-015-2900-1

Electrochemical deposition of gold on Indium zirconate ($InZrO_x$ with In/Zr atomic ratio: 1.0) for high temperature automobile exhaust gas sensors

Adeel Afzal,[*1,2,3] Mike Andersson,[4] Cinzia Di Franco,[5] Nicoletta Ditaranto,[1] Nicola Cioffi,[*1,6] Gaetano Scamarcio,[5,7] Anita Lloyd-Spetz,[4,8] Luisa Torsi[1,6]

[1] *Dipartimento di Chimica, Università degli Studi di Bari "Aldo Moro", via Orabona 4, Bari, 70126, Italy.*

[2] *Affiliated Colleges at Hafr Al-Batin, King Fahd University of Petroleum and Minerals, P.O. Box 1803, Hafr Al-Batin, 31991, Saudi Arabia.*

[3] *Department of Chemistry, University of Hafr Al-Batin, P.O. Box 1803, Hafr Al-Batin, 31991, Saudi Arabia.*

[4] *Division of Applied Sensor Science, Department of Physics, Chemistry and Biology, Linköping University, SE-581 83 Linköping, Sweden*

[5] *CNR-IFN U.O.S. Bari, via Amendola 173, Bari, 70126, Italy.*

[6] *TIRES Centro Interdipartimentale di Ricerca di Eccellenza, Università degli Studi di Bari "Aldo Moro", via Orabona 4, Bari, 70126, Italy.*

[7] *Dipartimento Interateneo di Fisica "M. Merlin", Università degli Studi di Bari "Aldo Moro", via Amendola 173, Bari, 70126, Italy.*

[8] *Microelectronics and Material Physics Laboratories, University of Oulu, FIN 900 14 Oulu, Finland.*

Corresponding authors: Tel.: +966 (0) 13 720 3426 x 1675 (AA); +39 080 544 2020 (NC).

Email addresses: aa@aafzal.com (AA); nicola.cioffi@uniba.it (NC).

Abstract

Automobile exhaust gas emissions are causing serious damage to urban air quality in and around major cities of the world, which demands continuous monitoring of exhaust emissions. The chief components of automobile exhaust include carbon monoxide (CO), nitrogen oxides (NO_x) and hydrocarbons. Indium zirconate ($InZrO_x$) and gold/indium zirconate ($Au/InZrO_x$) composite nanopowders are believed to be interesting materials to detect these substances. To this end, characterization and gas sensing properties of $InZrO_x$ and $Au/InZrO_x$ composite nanopowders are discussed. $InZrO_x$ nanoparticles with In/Zr atomic ratio of 1.00 (± 0.05) are synthesized via pH-controlled co-precipitation of In and Zr salts in aqueous ammonia. Gold (Au) nanoparticles are subsequently deposited on $InZrO_x$ using an *in situ* sacrificial Au electrolysis procedure. The products are characterized by scanning electron microscopy (SEM) and x-ray photoelectron spectroscopy (XPS). The gas sensing performance of $Au/InZrO_x$ composite nanopowder is studied by depositing a thick powder film on interdigitated electrode structures patterned on SiC substrate to facilitate high temperature operation. The resistivity of the $Au/InZrO_x$ layer is the sensor signal and the sensors could be operated at 500-600 °C, which is a suitable temperature range for engine exhaust measurements. The control sensing measurements reveal that $Au/InZrO_x$ composite nanopowder exhibits higher response towards 2-20 % O_2 gas as compared to pristine $InZrO_x$ nanoparticles. Further studies show that when applied to exhaust gases such as CO and nitric oxide (NO), the response of $Au/InZrO_x$ sensors is significantly higher towards NO in this temperature range. Thus, sensor performance characteristics of $Au/InZrO_x$ composite nanopowder are promising in terms of their applications in automobile exhaust emission control.

Keywords

Electrolysis; Exhaust emission control; Gas sensors; Gold; Indium zirconate; Nanomaterials

1. Introduction

The electronic gas sensors have found numerous applications in the past few decades including detection of hazardous combustible gases, industrial process and quality control, biomedical diagnostics, as well as monitoring automobile exhaust emissions [1]. Among these applications, detection of automobile exhaust gases specifically requires robust solid-state sensing devices that are stable and capable of withstanding harsh conditions such as temperature in the range of 500-600 °C [2–5]. Metal oxide based chemoresistive devices are particularly attractive for this purpose due to their simple structure, ease of fabrication, excellent miniaturization capability, ruggedness, and low cost [5, 6]. To date, a large number of metal oxides have been explored for their sensitivity towards various exhaust gases and they have been reviewed extensively in recent years [6–12].

In principal, the operation of chemoresistive devices is based on the changes in resistance, when they are exposed to varying concentrations of target analytes in the surrounding gaseous phase. This change in resistance in response to varying gas concentration is dependent on the partial pressure of surrounding oxygen in the gas phase and operating temperature [1, 3], as given below:

$$\boldsymbol{R_{\mathrm{sensor}} = P_{O_2}^{m} \cdot \exp\left(-{}^{E_a}/_{kT}\right)}$$

Where, R_{sensor} is the resistivity of the sensor; $\boldsymbol{P_{O_2}^{m}}$ is the partial pressure of oxygen; E_a is the activation energy for the conductivity; and T is the operating temperature.

Owing to the exponential dependence of chemoresistive sensors on temperature, the sensitivity to temperature variations presents a major challenge for these sensors, as described by Kim et al. [1] and therefore high performance temperature control of the sensor is important. In a recent critical review of the chemoresistive gas sensors, Sadek et al. [13] believe that dependence of sensor response on operating temperature originates from varying adsorption and desorption kinetics for oxygen ions on the oxide surfaces. The investigated material in this publication has a similar structure to the so called lambda sensor based on $YZrO_x$, for which oxygen ion diffusion through vacancies in the material and detection of the potential gradient over the material, constitutes the detection mechanism [14-16]. Therefore, also oxygen diffusion through vacancies in the $Au/InZrO_x$ may form at least part of the sensor detection mechanism.

In view of these limitations of the chemoresistive devices and to discover a novel metal/metal oxide nanocomposite system capable of sustaining high temperature operation and maintaining relatively constant response to various automobile exhaust gases, we hypothesize the use of indium zirconate ($InZrO_x$) and electrodecorated $Au/InZrO_x$ composite nanomaterials. Zirconia is one of the most commonly used O_2 and NO_x sensing material [14–16], whereas indium oxide is a semiconductor oxide that is recently being used as active material in exhaust gas sensors [17–19]. Furthermore, Au nanoparticles deposited on metal oxide supports are known to improve the catalytic activity and gas sensitivity of the oxide based nanomaterials [20–22]. Therefore, we employed an efficient electrochemical procedure to decorate nanoscale Au on the surface of

$InZrO_x$ in an anticipation to realize excellent gas sensing performance of Au/$InZrO_x$ composite nanoparticles at high temperatures.

2. Experimental

2.1. Materials

All chemicals were obtained from Sigma-Aldrich and used as received without further purification unless otherwise stated. These include indium chloride ($InCl_3$; 98%) zirconium oxychloride octahydrate ($ZrOCl_2.8H_2O$; ≥ 99.5%), silver nitrate ($AgNO_3$; 99.9999% crystalline solid), tetraoctylammonium chloride (TOAC; R_4NCl with R = C_8; ≥ 97%), tetrahydrofuran (THF; anhydrous; ≥ 99.9%) and acetonitrile (ACN; anhydrous; 99.8%). To remove traces of water (moisture), TOAC was vacuum dried for 4 h prior to use. For electrochemical synthesis, the electrodes were made of 0.25 mm thick gold and platinum foils (size: 25 × 25 mm; purity: 99.999%), which were purchased from Goodfellow. Both the electrodes were thoroughly cleaned with alumina powder, acetone, deionized water and acetone, respectively and dried under N_2 before use.

2.2. Methods

2.2.1. Preparation of indium zirconate ($InZrO_x$) nanoparticles

Indium zirconate ($InZrO_x$) nanoparticles were prepared via co-precipitation of an equimolar mixture of metal salts in liquid ammonia under controlled conditions of pH and temperature. Briefly, calculated amounts of $InCl_3$ and $ZrOCl_2.8H_2O$ were separately dissolved in 50 mL of double distilled deionized water to make two 0.05 M aqueous solutions. Both of these solutions were mixed while stirring, and warmed to 60 °C for 1 h. Subsequently, 0.05 M aqueous ammonia was added drop-wise to the reaction mixture to maintain the basic pH of 10. The mixture was aged for 2 h at 60 °C with continuous stirring. White precipitates of $InZrO_x$ were centrifuged, washed with double distilled deionized water to remove extra ammonia or unreacted species, if any, and dried under vacuum at room temperature.

2.2.2. Electrodecoration of $InZrO_x$ to prepare Au/$InZrO_x$ composite nanomaterials

As synthesized and dried $InZrO_x$ nanopowder was electrodecorated with gold (Au) nanoparticles using an *in situ* sacrificial Au anode electrolysis procedure [23]. The *in situ* electrodecoration of Au nanoparticles on $InZrO_x$ was performed in a three-electrode cell equipped with a solid Au working electrode (anode; area: 2.5 cm^2), a solid Pt counter electrode (cathode; area: 2.5 cm^2), and an $Ag/AgNO_3$ reference electrode (0.1 M $AgNO_3$ in ACN). The electrodes were immersed in 10 mL of 0.1 M electrolyte solution composed of vacuum dried TOAC in anhydrous THF/ACN (mixed in 3: 1 ratio). TOAC worked as the supporting electrolyte as well as the surfactant to stabilize Au nanoparticles. The solution was degassed for several minutes before use. 250 mg of

$InZrO_x$ powder were added to the electrolyte solution while stirring the mixture continuously to make a homogeneous mixture. The mixture was subsequently degassed for several minutes before the electrolysis. The sacrificial Au anode electrolysis was later executed in the potentiostatic mode with the potential difference of 1.5 V between the working and reference electrodes [24, 25]. The procedure was stopped after the accumulation of 100 C total charge. The amount of Au nanoparticles electrodecorated on the surface of $InZrO_x$ was calculated from the loss of mass by Au anode during the electrolytic process. $Au/InZrO_x$ composite nanoparticles were recovered by centrifugation at 6000 rpm and subsequently treated at 550 ˚C to remove organic species, adsorbed water, and surface -OH groups.

2.3. Characterization

2.3.1. X-ray photoelectron spectroscopy (XPS)

The surface analysis and chemical speciation of as synthesized $InZrO_x$ and $Au/InZrO_x$ nanoparticles was performed with X-ray photoelectron spectroscopy (XPS). An X-ray photoelectron Theta Probe spectrometer supplied by Thermo VG Scientific (West Sussex, England), equipped with micro-spot monochromatized Al Kα source was used for this purpose. Both wide scan and high resolution spectrum were obtained in a fixed analyzer transmission mode with pass energy of 150 and 100 eV, respectively. The XPS data were processed with the Avantage data system [26]. The binding energy (BE) scale was calibrated with reference to aliphatic C*1s* component at 284.8 ± 0.1 eV. The surface chemical composition of different samples was determined from the integrated areas of the principle photoelectron peaks and their sensitivity factors, as described elsewhere [27].

2.3.2. Scanning electron microscopy (SEM)

The surface morphology of $InZrO_x$ and $Au/InZrO_x$ nanoparticles was characterized with a field emission scanning electron microscope (FE-SEM), mod. ∑igma Zeiss. The samples were examined at 10-20 keV with 30 µm aperture and in-lens detector.

2.4. Device Structure, Fabrication, and Sensor Measurements

Interdigitated electrode structures were photolithographically patterned on an oxidized silicon wafer (Si/~800 Å SiO_2) followed by deposition of a double layer of 100 Å Ti and 3000 Å Au, and the finger electrodes were obtained through subsequent lift-off process. The distance between fingers was selected to be 40 µm. The wafer was then diced into individual chips, each with one interdigitated electrode structure of 2x2 mm size. After processing and dicing of the individual sensor chips, the chips were mounted onto alumina heater substrates together with an external Pt100 temperature sensor for heating and controlling the operation temperature of the sensors. The heater substrate, including the Pt100 temperature sensor, was attached to a TO8 header by spot welding. Electrical contact to the interdigitated electrode structures were made through gold wire bonding

with the pins on the TO8 header. Thus obtained miniaturized sensor set-up or device structure is shown in **Fig. S1** of the supporting information.

Both $InZrO_x$ and $Au/InZrO_x$ nanoparticles were deposited on the transducer structures in the form of a suspension. The suspensions were prepared by adding 200 µl of 99.5% ethanol to 50 µg of nanoparticles followed by 5 minutes of ultrasound sonication to make sure that a good concentration of nanoparticles was reached in the suspension. Each of these suspensions were deposited onto a set of four interdigitated electrode structures with the deposited amount being 2 µL in each case. This volume was selected as a result of a set of preliminary depositions and O_2 gas sensing measurements (data not shown), which indicated that in the series of deposited volumes of 2, 5, 10, and 20 µL, the smallest deposited volume (2 µL) returned the best sensor response. The sensor chips were heated to 75 °C during the deposition process, to evaporate ethanol more rapidly and ensure a uniform deposition of the nanoparticles. Thereafter, the devices were sintered at 600 °C in 20% O_2 in N_2 for 16 h to improve the mechanical and chemical stability of the sensing material and device for high temperature operation.

The resistance of the sensors was measured using a Keithly digital multimeter model 2001. Below 500°C the resistivity of the material exceeded 10 GOhm and was not possible to measure.

The control experiments were performed at 600 °C to evaluate the sensor characteristics of $InZrO_x$ and $Au/InZrO_x$ nanoparticles towards 2-20% O_2 concentrations in N_2 gas. Later, the practical gas sensing measurements were performed at 500-600 °C to study the sensor response of Au/InZrOx nanoparticles towards varying concentrations of automobile exhaust gases, i.e. nitric oxide (NO) and carbon monoxide (CO), in a constant background of 20% O_2 in N_2. The sensing measurements were carried out as follows: the device was exposed to 60 s pulses of test gas ranging from 40-400 ppm of NO or 100-1000 ppm of CO (one test gas at a time) followed by 120 s pulse of 20% O_2 in N_2. The normalized sensor response was calculated as the difference in resistance of the device under test gas and that measured in 20% O_2 in N_2 atmosphere, divided by the latter resistance value, as described elsewhere [28].

3. Results and Discussion

3.1. Electrochemical synthesis of $Au/InZrO_x$ composite nanoparticles

The electrochemical deposition of nanoscale Au on $InZrO_x$ nanopowder to form composite $Au/InZrO_x$ nanomaterials is achieved by sacrificial Au anode electrolysis. The set-up for electrochemical synthesis is shown in **Fig. 1a**, whereas the mechanism of Au nanoparticles' synthesis and deposition on $InZrO_x$ is shown in **Fig. 1b**. The electrochemical synthesis of $Au/InZrO_x$ nanoparticles in carried out at room temperature under inert atmosphere. As shown in Fig. 1b, the sacrificial Au anode is dissolved in the first step forming Au cations, which are stabilized by $InZrO_x$ nanoparticles present in the electrolyte solution through weak interactions between the Au^+ ions and hydroxyl (-OH) groups disposed on the surface of $InZrO_x$ nanoparticles [29, 30]. In the next step,

these stabilized or supported Au^+ ions are reduced to nanoscale Au at Pt cathode. Certain Au^+ species may also wander freely in the solution before forming Au ad-atoms at the surface of cathode. These ad-atoms form free Au nanoparticles, which may subsequently be stabilized by the supporting electrolyte (TOAC) as well as by $InZrO_x$. In our previous experiments, it has been found that only a small amount (~2 wt%) of Au nanoparticles are lost during the electrolysis and subsequent recovery steps [31]. Finally, $Au/InZrO_x$ composite nanoparticles are recovered by centrifugation, dried, and thermally treated at 550 °C for potential high temperature gas sensor applications.

3.2. Characterization: Surface Analysis

Surface analytical characterization of pristine $InZrO_x$ and $Au/InZrO_x$ composite nanoparticles is performed by XPS to study the surface chemical speciation and the elemental state of In, Zr, and Au. The detailed chemical composition of $InZrO_x$ and $Au/InZrO_x$ nanoparticles is given in **Table 1**, while **Fig. 2** shows the high resolution photoelectron spectra of different elements of interest in both samples. All of the following signals: C*1s*, In*3d*, Zr*3d*, O*1s*, and Cl*2p* are found in the wide or survey scans of both samples, while Au*4f* is found only in $Au/InZrO_x$ nanoparticles that is obvious. The presence of C*1s* is attributed to organic impurities, to CO/CO_2 gases adsorbed on the surface of these nanomaterials, and to quaternary ammonium species, in the case of $Au/InZrO_x$. Cl*2p* comes from the counter ions formed during the co-precipitation reaction for synthesis of $InZrO_x$ nanoparticles, whereas in case of $Au/InZrO_x$ nanoparticles, it belongs to the TOAC molecules used as electrolyte and surfactant during the electrolysis procedure.

Figure 2 & Table 1 here

O*1s*, In*3d* and Zr*3d* are present in both samples. Interestingly, the relative abundance of In and Zr in $InZrO_x$ sample is same that indicates the formation of $Au/InZrO_x$ nanoparticles with In/Zr atomic ratio of 1.08 via co-precipitation of the equimolar $InCl_3$ and $ZrOCl_2.8H_2O$ solutions. In addition, when $InZrO_x$ nanopowders are subjected to an *in situ* electrodecoration procedure, the resulting $Au/InZrO_x$ composite nanoparticles also possess similar abundance with In/Zr atomic ratio of 0.97, which is very close to the actual In/Zr ratio in pristine $Au/InZrO_x$. The small difference between the experimental atomic ratios is within the uncertainty of this calculation. Nevertheless, a slight variation in relative atomic percentages of In and Zr in two samples may be attributed to the dissolution and re-precipitation phenomenon [32, 33] of oxide nanoparticles during the course of electrolysis. Moreover, the In-O signal in as prepared InZrOx is positively shifted by 0.7 eV (BE=445.1±0.1 eV) respect to thermally annealed Au/InZrOx (BE=444.4±0.1 eV), which is ascribable to non-stoichiometric indium oxides [34].

Another distinguishing feature in surface characterization of two samples ($InZrO_x$ and $Au/InZrO_x$) is observed to be the O/M ratio (At%). The O/M ratio can be calculated from the data reported in Table 1. In case of pristine $InZrO_x$ nanoparticles, the O/M ratio is found to be 2.53, which is an indicative of the presence of a large number of hydroxyl (-OH) groups on the surface of as synthesized $InZrO_x$. On the other hand, $Au/InZrO_x$ samples exhibit very low O/M ratio, i.e. 1.98, probably due to thermal treatment at 550 °C. Such low O/M ratio might also indicate the formation of defects or oxygen vacancies in $Au/InZrO_x$ composite nanoparticles as a consequence of thermal

annealing [35–37]. These oxygen vacancies in oxide nanoparticles are believed to be adsorption-active sites that enhance overall catalytic and gas sensing performance of the nanomaterials [38–40]. The high resolution photoelectron spectrum of Au*4f* shows the presence of Au in two chemical states of which a great majority is found as elemental gold (Au^0) nanoparticles, i.e. 1.0±0.2 At%, while a small proportion (i.e. 0.1 At%), is under the form of Au^{3+} oxide, on the surface of Au/$InZrO_x$ nanoparticles. The BE value of nanosized elemental gold is systematically below that expected for metallic bulk gold (84.0 eV), and this is interpreted in terms of initial state effects [41], although the occurrence of a strong electronic interaction between gold and the Indium Zirconate, i.e., electron transfer to gold, cannot ruled out and might concur to the observed chemical shift, as well.

3.3. Characterization: Morphology

The morphology of pristine $InZrO_x$ and electrodecorated Au/$InZrO_x$ composite nanoparticles is shown in **Fig. 3**. $InZrO_x$ is synthesized as nanopowder, and electrodecorated via sacrificial Au anode electrolysis. Nanosized $InZrO_x$ powder is visible in the respective SEM image (see Fig. 2a). The electrolysis process is known to yield Au nanoparticles with an average size < 10 nm [24, 41]. Moreover, it has already been established that Au nanoparticles' size distribution range is narrow depending upon the nature of surfactant [41]. Herein, Au nanoparticles deposited on the surface of $InZrO_x$ can be clearly observed in Fig. 2b. It is important to mention that the image is obtained after thermal annealing of the Au/$InZrO_x$ composite nanomaterials at 550 °C. Nanoscale Au particles can be identified individually on the surface, which further confirms the results obtained from XPS surface analysis. The presence of individual Au nanoparticles also signifies the effective stabilization by TOAC and oxide support. As discussed above, pristine or as synthesized $InZrO_x$ nanopowders are subjected to electrolytic deposition of Au due to the enriched presence of surface hydroxyl groups on oxide support that favors efficient deposition of Au nanoparticles on metal oxide supports [23].

Figure 3 here

3.4. Control Measurements: $InZrO_x$ vs. Au/$InZrO_x$ Nanoparticles

In our preliminary experiments, the device is exposed to different concentrations of O_2 in N_2 to measure the sensor characteristics of $InZrO_x$ and Au/$InZrO_x$ nanoparticles under harsh conditions. The results from these control measurements performed at 600 °C are shown in **Fig. 4.** It can be seen that pristine $InZrO_x$ nanoparticles exhibit very high resistance and the level of the noise is fairly high. Moreover, there is no significant change that can be undoubtedly attributed to the variations in gas concentration, i.e. any straightforward sensor pattern is not observed for pristine $InZrO_x$ nanoparticles. It is therefore not possible to really evaluate $InZrO_x$ films in terms of gas sensitivity. Au/$InZrO_x$ nanoparticles, on the other hand, exhibit significant variations in resistance, when exposed to different pulses of varying oxygen concentration. Only a temperature range of 500-600°C has been evaluated since the resistance even of the gold decorated material is too high (> 10 GOhm) at lower temperatures. However, it is obvious that electrodecoration of InZrOx with

Au nanoparticles improves gas sensitivity under harsh conditions. This observation is partially supported by previous work on Au-doped or un-doped indium and-or zirconium oxide based gas sensors [22, 42]. Consequently, the results reported herein for the rest of the gas (NO and CO) sensing tests are for electrodecorated Au/InZrOx composite nanoparticles.

Figure 4 here

3.5. NO and CO Sensor Characteristics of Au/InZrO$_x$ Nanoparticles

The objective of developing electrodecorated Au/InZrO$_x$ composite nanoparticles is to test their high temperature sensing properties for automobile exhaust pollutants such as NO and CO. Thus, NO and CO gases are used as target analytes for a preliminary evaluation of the mentioned Au/InZrO$_x$ nanomaterials as active layers in automotive applications. The sensing measurements are carried out at 500 and 600 °C operation temperatures. **Fig. 5** shows the absolute as well as the normalized sensor responses to different concentrations of NO (ranging from 40-400 ppm) in a constant background of 20% O_2 in N_2. While for Au/InZrO$_x$ sensor, the absolute resistance changes are significantly larger at the lower temperature (as reported in Fig. 5a**)**, the normalized responses recorded at higher NO concentrations are only marginally higher at 500 °C. Nonetheless, there is not much difference in magnitude of the normalized or relative response of Au/InZrO$_x$ sensor towards different concentrations of NO at the two different operation temperatures. The dynamic range seems to be about 50 – 400 ppm NO. The repeated measurements during 30 minutes indicates that the Au/InZrO$_x$ nanoparticle film is stable even in exposure to NO at these high temperatures. However, long term testing, also in humid atmosphere, is necessary to show if this material is promising for automotive applications.

Figure 5 here

The absolute and normalized sensor responses of Au/InZrO$_x$ films towards varying concentrations of CO (ranging from 100-1000 ppm) in a constant background of 20% O_2 in N_2 are reported in **Fig. 6.** The results indicate that in contrast to their response towards NO gas concentrations, the normalized sensor responses are greater at the higher operation temperature, i.e. 600 °C. Also contrary to Au/InZrOx sensor's response to NO, the dynamic range for the normalized sensor responses to CO is much higher, about 100 – 700 ppm for both operation temperatures. The results indicate non-linear response characteristics and higher effect of temperature for the CO sensitivity of the Au/InZrO$_x$ sensor. The results are further discussed below giving a comparison of the sensitivity of Au/InZrO$_x$ sensor towards different gases and other sensor characteristics.

Figure 6 here

3.6. Statistical analysis

The gas sensing performance of Au/InZrO$_x$ sensor is further explored by statistical analysis of the sensor results. A comparison of the absolute sensor responses of Au/InZrO$_x$ towards different concentrations of NO and CO gases at 500 °C is drawn in **Fig. 7**. The different concentration ranges for the two gases are chosen as relevant for real conditions in automotive exhausts. Visibly,

the material exhibits a significantly higher response towards relatively lower concentrations of NO as compared to CO. In other terms, if similar concentrations of NO and CO are considered, the sensor shows severalfold higher response towards NO as compared to CO, which suggests that at lower concentrations of NO and CO gases, the Au/$InZrO_x$ sensor could be used as a selective NO sensor with low cross sensitivity to CO. Moreover, the Au/$InZrO_x$ sensor shows promising fast response and recovery kinetics with t_{res90} reached within 60 s in Figs. 5 b and 6 b at 600 °C and t_{rec90} reached within 60 s in Fig. 5 b at 500°C and in Fig. 6 b, at both temperatures.

Figure 7 here

Overall sensitivity of the Au/$InZrO_x$ sensor towards tested gases (NO and CO) is determined by plotting the normalized sensor responses as a function of different gas concentrations, as shown in **Fig. S2**. In case of NO gas, the Au/$InZrO_x$ sensor shows linear response in the concentration range of 40-160 ppm, which gets little saturated at higher concentrations of 200-400 ppm. The slope of the linear NO response range shows a sensitivity factor of ~2000 Ω ppm^{-1} for Au/$InZrO_x$ nanomaterials. On the contrary, the normalized sensor response towards varying concentrations of CO is not exactly linear in any concentration range. The relatively straight line obtained in the concentration range of 200-500 ppm CO shows poor sensitivity of the Au/$InZrO_x$ nanoparticle-sensor towards CO with a factor of ~50 Ω ppm^{-1}. Thus, electrodecorated Au/$InZrO_x$ composite nanoparticles show 40 times higher sensitivity towards NO compared with that of CO. These results suggest that Au/$InZrO_x$ is an interesting candidate for nitric oxide (NO) detection in automobile exhaust under harsh conditions. Additional tests with other interferent species are planned, as well as long-term stability evaluations under humid conditions.

4. Conclusions

$InZrO_x$ nanoparticles with In/Zr atomic ratio of 1.0 are obtained via co-precipitation of equimolar salt solutions. The resulting $InZrO_x$ nanoparticles are electrodecorated with nanoscale Au using an *in situ* sacrificial anode electrolysis procedure. Both $InZrO_x$ and Au/$InZrO_x$ nanoparticles are subsequently characterized and deposited on miniaturized electronic devices for high temperature gas sensing measurements. The preliminary experiments reveal that pristine $InZrO_x$ nanoparticles are not active, while electrodecoration of nanoscale Au considerably enhances the performance of Au/$InZrO_x$ nanoparticles. High temperature NO and CO sensing results demonstrate higher absolute and normalized sensor response of Au/$InZrO_x$ nanoparticles towards 40-400 ppm NO. At an operation temperature of 500°C, the Au/$InZrO_x$ sensors exhibit 40 fold higher sensitivity towards NO as compared to CO. Furthermore, the Au/$InZrO_x$ sensor shows response and recovery times and stability towards storage, which is promising for applications in harsh conditions.

Acknowledgements

This manuscript is designed for the special issue devoted to the anniversary of Professor M. A. Vorotyntsev.

Authors gratefully acknowledge the Apulian Technological District on Mechatronics (MEDIS) and the Italian Ministero dell'Istruzione, dell'Universita e della Ricerca (MIUR), PON program 2007–2013 for financial support.

References

1. Kim I-D, Rothschild A, Tuller HL (2013) Advances and new directions in gas-sensing devices. Acta Mater 61:974–1000

2. Riegel J, Neumann H, Wiedenmann H-M (2002) Exhaust gas sensors for automotive emission control. Solid State Ion 152:783–800.

3. Moos R (2005) A Brief Overview on Automotive Exhaust Gas Sensors Based on Electroceramics. Int J Appl Ceram Technol 2:401–413.

4. Moos R (2010) Catalysts as Sensors—A Promising Novel Approach in Automotive Exhaust Gas Aftertreatment. Sensors 10:6773–6787.

5. Moos R (2011) New Approaches for Exhaust Gas Sensing. In: Fleischer M, Lehmann M (eds) Solid State Gas Sens. - Ind. Appl. Springer Berlin Heidelberg, pp 173–188

6. Afzal A, Cioffi N, Sabbatini L, Torsi L (2012) NOx sensors based on semiconducting metal oxide nanostructures: Progress and perspectives. Sens Actuators B Chem 171-172:25–42.

7. Lutic D, Strand M, Lloyd-Spetz A, Buchholt K, Ieva E, Käll P-O, Sanati M (2007) Catalytic properties of oxide nanoparticles applied in gas sensors. Top Catal 45:105–109

8. Barsan N, Koziej D, Weimar U (2007) Metal oxide-based gas sensor research: How to? Sens Actuators B Chem 121:18–35.

9. Du N, Zhang H, Chen BD, Ma XY, Liu ZH, Wu JB, Yang DR (2007) Porous indium oxide nanotubes: Layer-by-layer assembly on carbon-nanotube templates and application for room-temperature NH_3 gas sensors. Adv Mater 19:1641–1645

10. Liu X, Zhang J, Wang L, Yang T, Guo X, Wu S, Wang S (2011) 3D hierarchically porous ZnO structures and their functionalization by Au nanoparticles for gas sensors. J Mater Chem 21:349–356

11. Fleischer M, Lehmann M (2012) Solid State Gas Sensors - Industrial Application. Springer Berlin Heidelberg, Berlin, Heidelberg

12. Huotari J, Lappalainen J, Puustinen J, Lloyd Spetz A (2013) Gas sensing properties of pulsed laser deposited vanadium oxide thin films with various crystal structures. Sens Actuators B Chem 187:386–394.

13. Sadek AZ, Choopun S, Wlodarski W, Ippolito SJ, Kalantar-Zadeh K (2007) Characterization of ZnO Nanobelt-Based Gas Sensor for H_2, NO_2, and Hydrocarbon Sensing. IEEE Sens J 7:919–924

14. Cho H-C, Takase S, Song J-H, Shimizu Y (2013) Sensing behavior of solid-state impedancemetric NOx sensor using solid electrolyte transducer and oxide receptor. Sens Actuators B Chem 187:94–98.

15. Cui L, Han F, Dai W, Murray EP (2014) Influence of Microstructure on the Sensing Behavior of NOx Exhaust Gas Sensors. J Electrochem Soc 161:B34–B38.

16. Maskell WC, Brett DJL, Brandon NP (2014) Thick-film amperometric zirconia oxygen sensors: influence of cobalt oxide as a sintering aid. Meas Sci Technol 25:065104.

17. Sowti khiabani P, Marzbanrad E, Hassani H, Raissi B (2013) Fast Response NO_2 Gas Sensor Based on In2O3 Nanoparticles. J Am Ceram Soc 96:2493–2498.

18. Kim B-J, Song I-G, Kim J-S (2014) In_2O_3-based micro gas sensor for detecting NO x gases. Electron Mater Lett 10:509–513.

19. Yang W, Wan P, Zhou X, Hu J, Guan Y, Feng L (2014) Additive-Free Synthesis of In_2O_3 Cubes Embedded into Graphene Sheets and Their Enhanced NO_2 Sensing Performance at Room Temperature. ACS Appl Mater Interfaces 6:21093–21100

20. Ivanovskaya MI, Ovodok EA, Kotsikau DA (2012) Interaction of carbon monoxide with In2O3 and In2O3-Au nanocomposite. J Appl Spectrosc 78:842–847.

21. Karwacki CJ, Ganesh P, Kent PRC, Gordon WO, Peterson GW, Niu JJ, Gogotsi Y (2013) Structure–activity relationship of Au/ZrO_2 catalyst on formation of hydroxyl groups and its influence on CO oxidation. J Mater Chem A 1:6051–6062

22. Li X, Liu J, Guo H, Zhou X, Wang C, Sun P, Hu X, Lu G (2014) $Au@In_2O_3$ core–shell composites: a metal–semiconductor heterostructure for gas sensing applications. RSC Adv 5:545–551

23. Afzal A, Di Franco C, Mesto E, Ditaranto N, Cioffi N, Scordari F, Scamarcio G, Torsi L (2015) Au/In_2O_3 and Au/ZrO_2 composite nanoparticles via in situ sacrificial gold electrolysis. Mater Express accepted for publication.

24. Reetz MT, Helbig W (1994) Size-selective synthesis of nanostructured transition metal clusters. J Am Chem Soc 116:7401–7402.

25. Reetz MT, Quaiser SA (1995) A new method for the preparation of nanostructured metal clusters. Angew Chem Int Ed Engl 34:2240–2241. doi: 10.1002/anie.199522401

26. Thermo Avantage (2012) Avantage Data System. Thermo Fisher Scientific Inc.

27. Pilolli R, Ditaranto N, Franco C, Palmisano F, Cioffi N (2012) Thermally annealed gold nanoparticles for surface-assisted laser desorption ionisation–mass spectrometry of low molecular weight analytes. Anal Bioanal Chem 404:1703–1711

28. Pearce R, Iakimov T, Andersson M, Hultman L, Spetz AL, Yakimova R (2011) Epitaxially grown graphene based gas sensors for ultra sensitive NO_2 detection. Sens Actuators B Chem 155:451–455

29. Stefánsson A (2002) The stability and stoichiometry of gold(I) and silver(I) complexes in hydrothermal solutions /. Swiss Federal Institute of Technology, Zurich

30. Huang Y, Li D, Li J (2004) β-Cyclodextrin controlled assembling nanostructures from gold nanoparticles to gold nanowires. Chem Phys Lett 389:14–18.

31. Monopoli A, Afzal A, di Franco C, Ditaranto N, Cioffi N, Nacci A, Cotugno P, Torsi L (2014) Design of novel indium oxide supported gold nanocatalysts and their application in homocoupling of arylboronic acids. J Mol Catal Chem 386:101–107

32. Yang H, Wang S, Yang Y (2012) Zn-doped In_2O_3 nanostructures: preparation, structure and gas-sensing properties. CrystEngComm 14:1135–1142.

33. Rich R (2007) Inorganic Reactions in Water. Springer

34. Lin AWC, Armstrong NR, Kuwana T (1977) X-ray photoelectron/Auger electron spectroscopic studies of tin and indium metal foils and oxides Anal Chem 49: 1228–1235

35. Fabris S, Paxton AT, Finnis MW (2002) A stabilization mechanism of zirconia based on oxygen vacancies only. Acta Mater 50:5171–5178.

36. Agoston P, Albe K, Nieminen RM, Puska MJ (2009) Intrinsic n-type behavior in transparent conducting oxides: a comparative hybrid-functional study of In_2O_3, SnO_2, and ZnO. Phys Rev Lett 103:245501.

37. Mahmood Q, Afzal A, Siddiqi HM, Habib A (2013) Sol–gel synthesis of tetragonal ZrO_2 nanoparticles stabilized by crystallite size and oxygen vacancies. J Sol-Gel Sci Technol 67:670–674.

38. Borisenko VE, Gaponenko SV, Gurin VS (2011) Physics, Chemistry and Applications of Nanostructures: Proceedings of the International Conference Nanomeeting--2011 : Reviews and Short Notes : Minsk, Belarus, 26-29 May 2009. World Scientific

39. Ye J, Liu C, Mei D, Ge Q (2013) Active Oxygen Vacancy Site for Methanol Synthesis from CO2 Hydrogenation on In_2O_3(110): A DFT Study. ACS Catal 3:1296–1306.

40. Gan J, Lu X, Wu J, Xie S, Zhai T, Yu M, Zhang Z, Mao Y, Wang SCI, Shen Y, Tong Y (2013) Oxygen vacancies promoting photoelectrochemical performance of In_2O_3 nanocubes. Sci Rep 3:Art. No. 1021

41. Cioffi N, Colaianni L, Ieva E, Pilolli R, Ditaranto N, Angione MD, Cotrone S, Buchholt K, Spetz AL, Sabbatini L, Torsi L (2011) Electrosynthesis and characterization of gold nanoparticles for electronic capacitance sensing of pollutants. Electrochimica Acta 56:3713–3720

42. Baltrus JP, Ohodnicki PR, Joy NA, Carpenter MA (2014) Examination of charge transfer in Au/YSZ for high-temperature optical gas sensing. Appl Surf Sci 313:19–25.

Figure Captions

Fig. 1. (a) The experimental set-up for synthesis of electrodecorated Au/$InZrO_x$ composite nanoparticles. (b) A representation of the proposed mechanism of the electrodecoration procedure for synthesis of Au/$InZrO_x$ composite nanoparticles.

Fig. 2. The surface chemical analysis of pristine $InZrO_x$ and electrodecorated Au/$InZrO_x$ nanoparticles by x-ray photoelectron spectroscopy (XPS): The representative high resolution XPS spectra of In*3d*, Zr*3d*, O*1s*, and Au*4f* regions are shown for different samples, respectively.

Fig. 3. SEM images of pristine $InZrO_x$ nanoparticles (a) and electrodecorated Au/$InZrO_x$ composite nanoparticles (b).

Fig. 4. The response characteristics of pristine $InZrO_x$ and electrodecorated Au/$InZrO_x$ nanoparticles applied to interdigitated electrode structures towards 2-20% O_2 in N_2 at 600 °C.

Fig. 5. A comparison of the absolute (a) and normalized (b) sensor responses to 40-400 ppm NO gas for the Au/$InZrO_x$ sensors at 500 and 600°C operation temperature. Absolute resistance changes were comprised between 5 and 40 MΩ.

Fig. 6. A comparison of the absolute (a) and normalized (b) sensor responses to 100-1000 ppm CO gas for the Au/$InZrO_x$ sensors at 500 and 600°C operation temperature. Absolute resistance changes were comprised between 5 and 35 MΩ.

Fig. 7. A Comparison of the Au/$InZrO_x$ sensor's response towards different concentrations of NO and CO gases at 500 °C operation temperature.

Tables

Table 1. XPS surface chemical speciation of pristine $InZrO_x$ and electrodecorated $Au/InZrO_x$ composite nanoparticles. Data are averaged out three replicates (n=3) and reported as mean value ± 1 standard deviation.

Peak	*Attribution*	*As prepared InZrO$_x$*		*Thermally treated Au/InZrO$_x$*	
		BE (eV)	At%	BE (eV)	At%
C1s	C–C	284.8±0.1	19±3	284.8±0.1	14.0±1.0
	C–O	286.4±0.1	7±2	286.4±0.1	3.2±0.5
	C=O	288.8±0.1	3.0±0.8	288.8±0.1	1.5±0.5
Au4f$_{7/2}$	Au^0	-	-	83.2±0.1	1.0±0.2
	Au^{3+}	-	-	84.6±0.4	0.1±0.2
In3d$_{5/2}$	In–O	445.1±0.1	9.3±0.2	444.4±0.1	11.4±0.2
Zr3d$_{5/2}$	Zr–O	182.3±0.1	8.6±0.6	182.1±0.1	11.7±0.2
O1s	O–In/O–Zr	530.2±0.1	12.2±1.1	530.1±0.1	34.6±1.0
	O–In/O–Zr, C=O	531.7±0.1	30±4	531.6±0.1	11.1±1.6
	O–C, loosely bound O	533.4±0.2	6±4	532.9±0.2	4.0±0.5
Cl2p$_{3/2}$	Cl-C, Cl^-	198.7±0.1	5.3±0.6	198.8±0.1	7.3±0.6

Figure 1

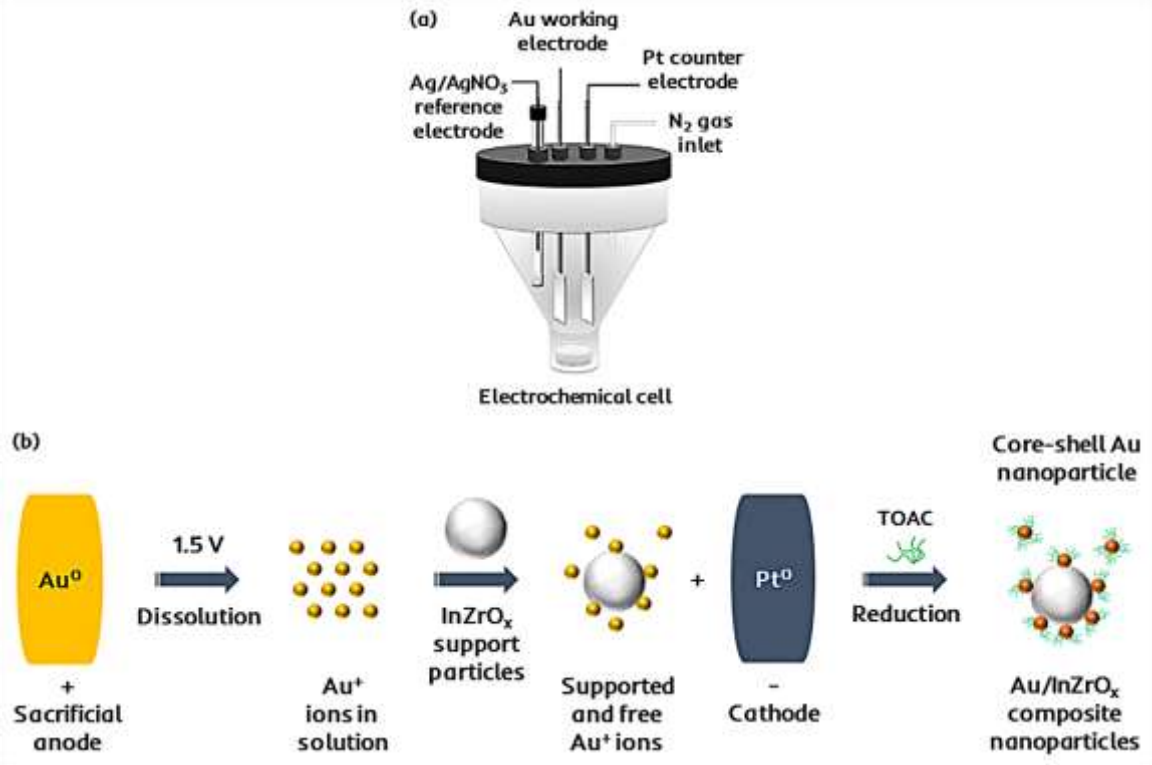
(a)
Au working electrode
Pt counter electrode
Ag/AgNO3 reference electrode
N2 gas inlet
Electrochemical cell
(b)
Core-shell Au nanoparticle
Au0
1.5 V
Dissolution
InZrOx support particles
Pt0
TOAC
Reduction
+
Sacrificial anode
Au+ ions in solution
Supported and free Au+ ions
-
Cathode
Au/InZrOx composite nanoparticles

Figure 2

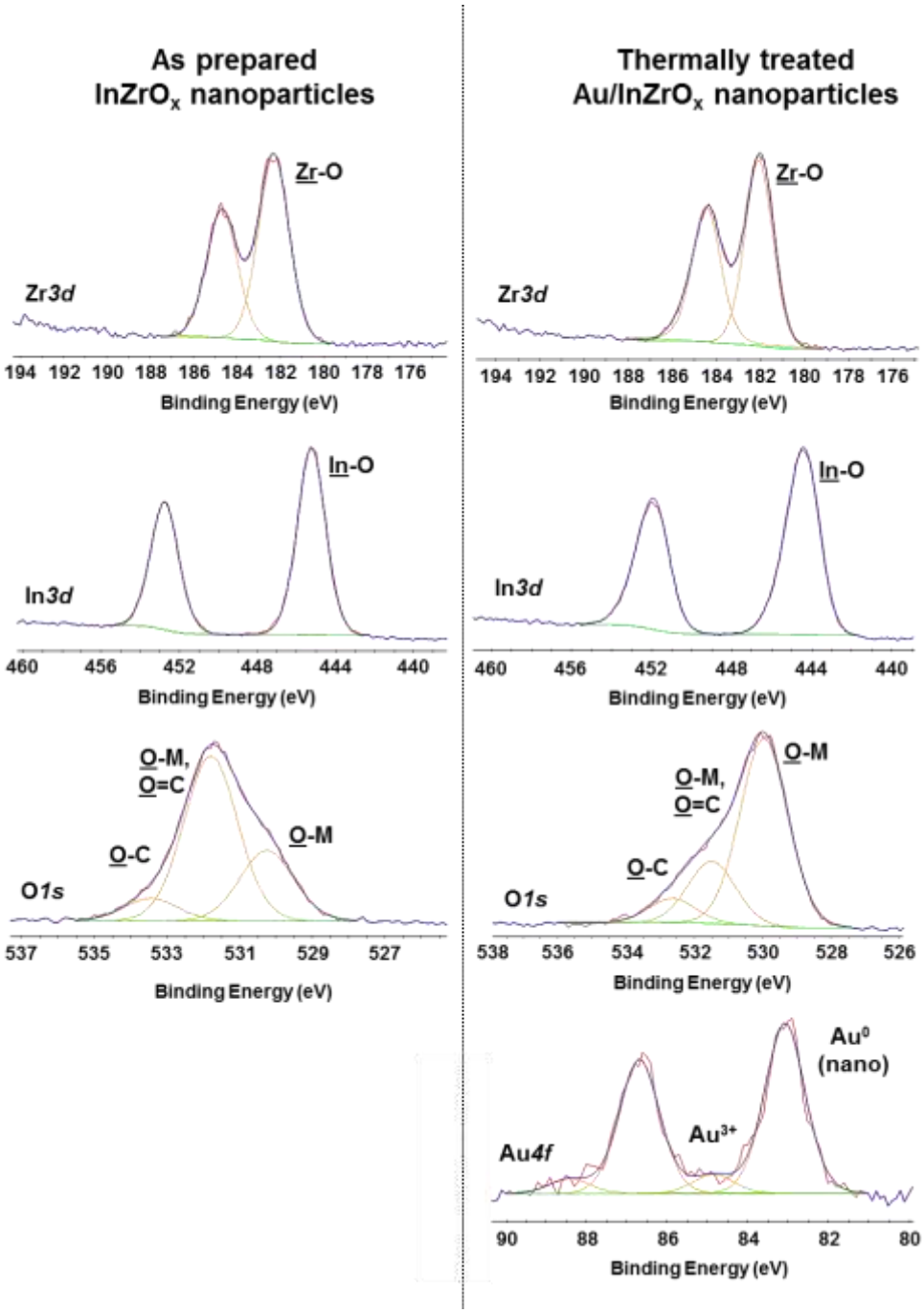
As prepared
InZrO$_x$ nanoparticles
Thermally treated
Au/InZrO$_x$ nanoparticles
Zr-O
Zr3d
194 192 190 188 186 184 182 180 178 176
Binding Energy (eV)
In-O
In3d
460 456 452 448 444 440
Binding Energy (eV)
O-M,
O=C
O-C
O-M
O1s
537 535 533 531 529 527
Binding Energy (eV)
538 536 534 532 530 528 526
Au^0
(nano)
Au^{3+}
Au4f
90 88 86 84 82 80

Figure 3

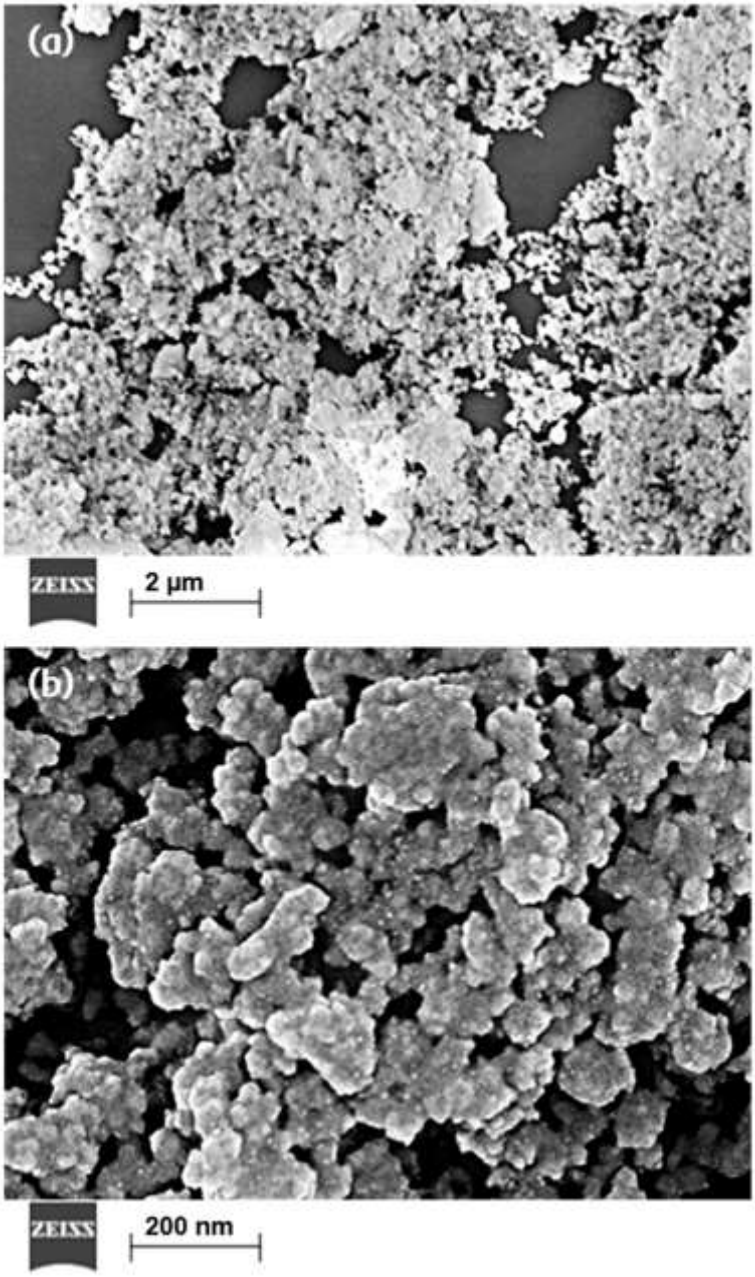

Figure 4

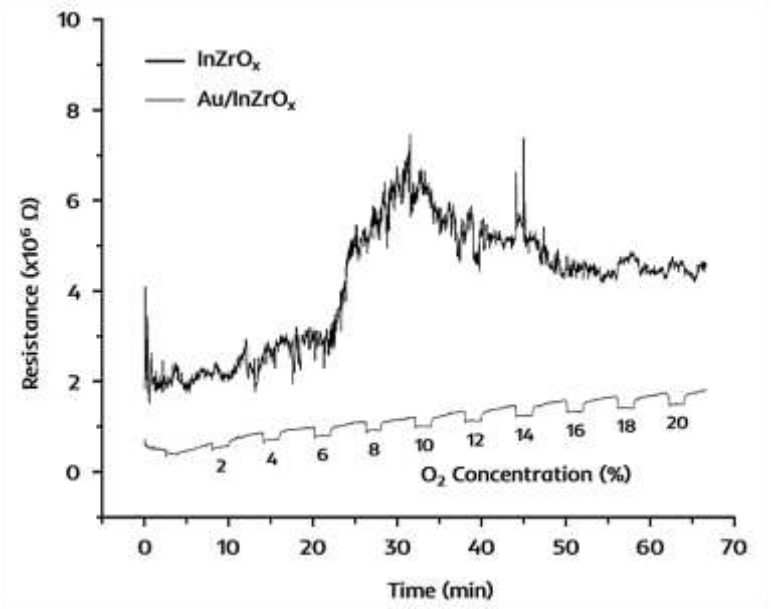
InZrO$_x$
Au/InZrO$_x$
Resistance (x10^6 Ω)
10
8
6
4
2
0
2
4
6
8
10
12
14
16
18
20
O$_2$ Concentration (%)
0
10
20
30
40
50
60
70
Time (min)

Figure 5

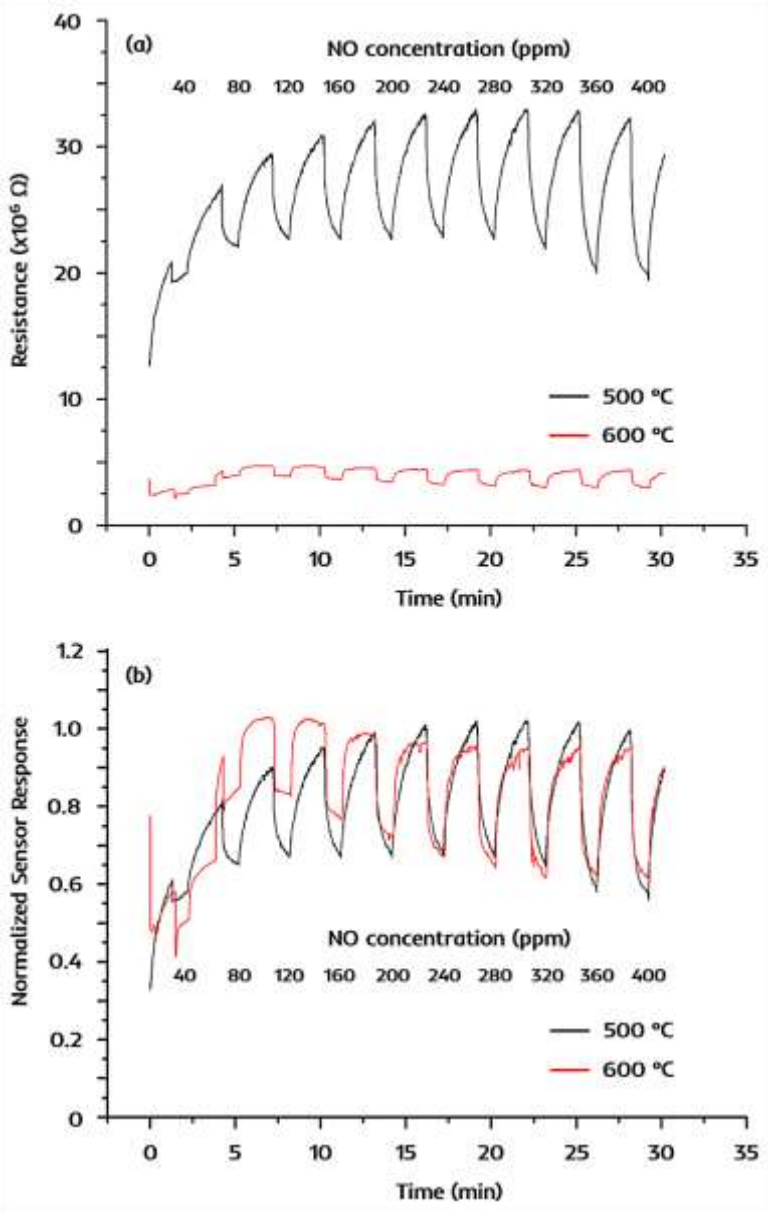
(a)
NO concentration (ppm)
40 80 120 160 200 240 280 320 360 400
Resistance (x10⁶ Ω)
500 °C
600 °C
Time (min)
(b)
Normalized Sensor Response
NO concentration (ppm)
40 80 120 160 200 240 280 320 360 400
500 °C
600 °C
Time (min)

Figure 6

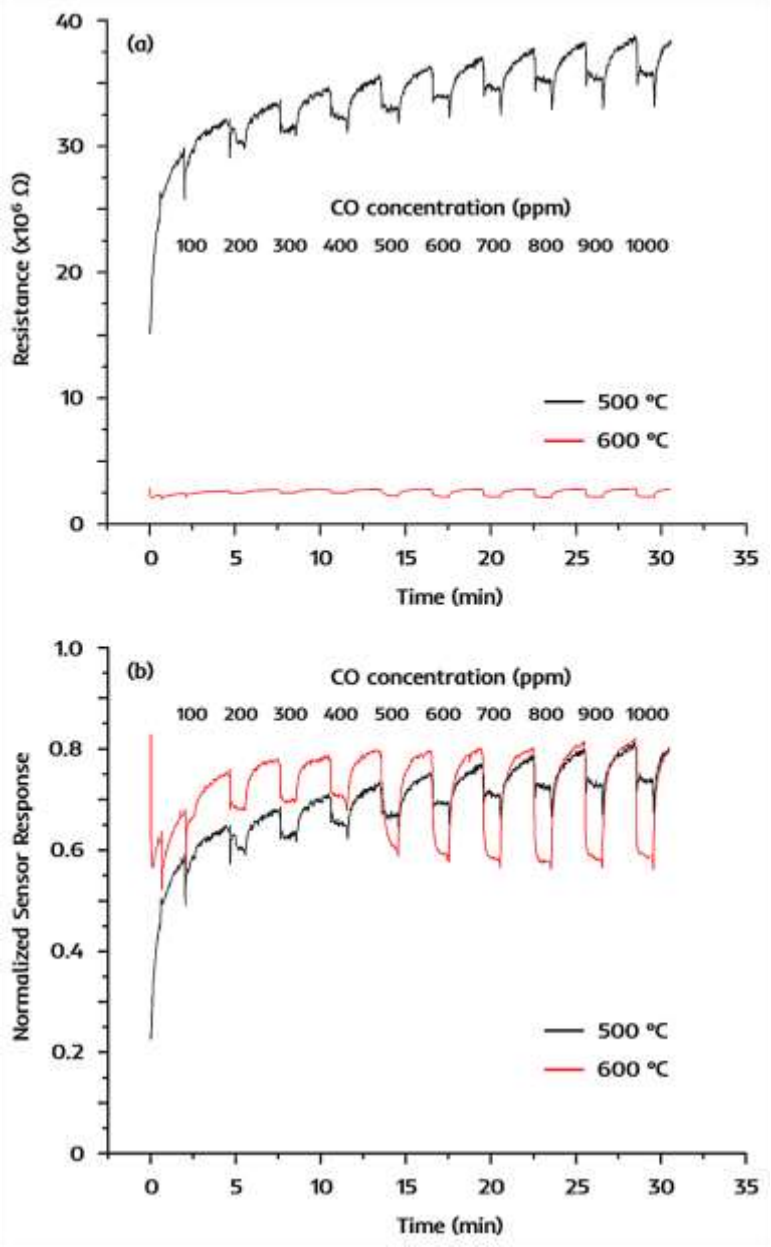
(a)
Resistance (x10⁶ Ω)
CO concentration (ppm)
100 200 300 400 500 600 700 800 900 1000
500 °C
600 °C
Time (min)
(b)
Normalized Sensor Response
CO concentration (ppm)
100 200 300 400 500 600 700 800 900 1000
500 °C
600 °C
Time (min)

Figure 7

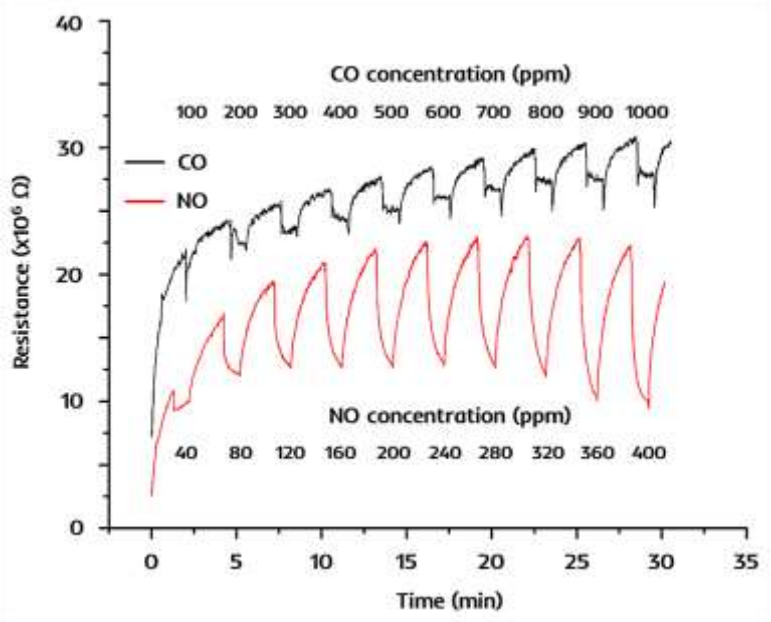
CO concentration (ppm)
100 200 300 400 500 600 700 800 900 1000
CO
NO
NO concentration (ppm)
40 80 120 160 200 240 280 320 360 400
Resistance (x10⁶ Ω)
Time (min)
0 5 10 15 20 25 30 35
0 10 20 30 40

Electrochemical deposition of gold on Indium zirconate ($InZrO_x$ with In/Zr atomic ratio: 1.0) for high temperature automobile exhaust gas sensors

Adeel Afzal,[*1,2,3] Mike Andersson,[4] Cinzia Di Franco,[5] Nicoletta Ditaranto,[1] Nicola Cioffi,[*1,6] Gaetano Scamarcio,[5,7] Anita Lloyd-Spetz,[4,8] Luisa Torsi[1,6]

Supporting Information

Fig. S1. The structure of device showing the sensor chip with finger electrodes and a Pt100 temperature sensor mounted on the same heater substrate through a high temperature die attachment, and electrically connected to the 16-pin TO8 header through gold wire bonding.

Fig. S2. Statistical analysis of the Au/$InZrO_x$ based sensor's response towards different concentrations of NO (a) and CO (b) gases at 500 °C. The insets show linear response range for NO.

Figure S1

Figure S2

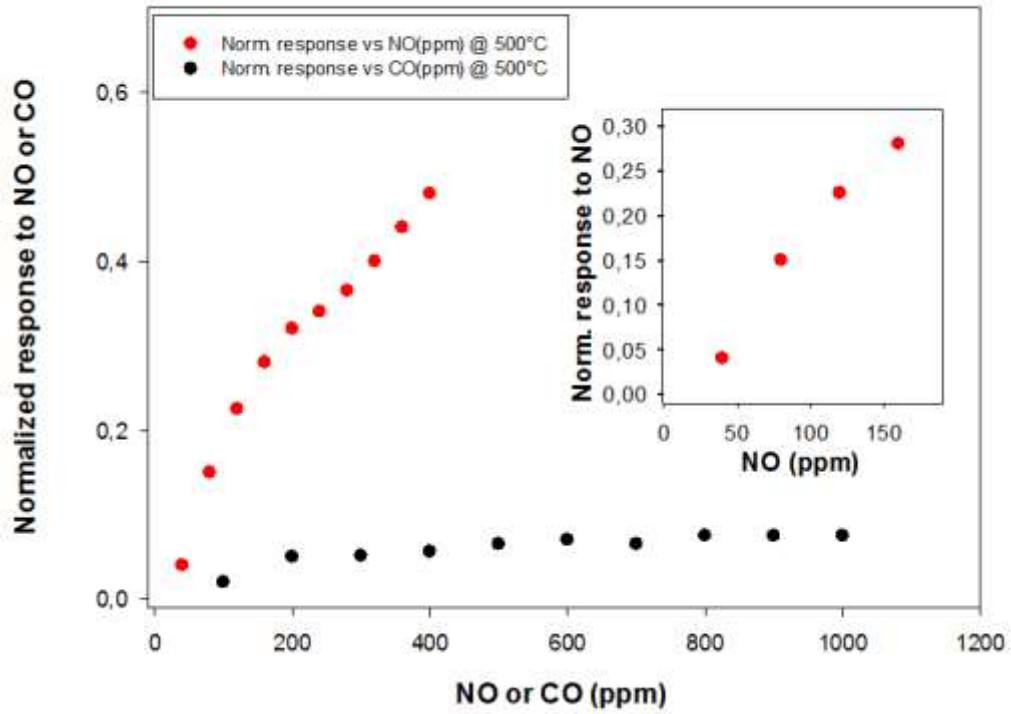
Norm. response vs NO(ppm) @ 500°C
Norm. response vs CO(ppm) @ 500°C
Normalized response to NO or CO
NO or CO (ppm)
0,0
0,2
0,4
0,6
0
200
400
600
800
1000
1200
Norm. response to NO
NO (ppm)
0,00
0,05
0,10
0,15
0,20
0,25
0,30
0
50
100
150